

## Melt crystallization of ibuprofen on surfaces patterned by a Nd : YAG laser

Jihae Chung\*, Byung Jick Kim\*, Haseung Chung\*\*, and Il Won Kim\*<sup>†</sup>

\*Department of Chemical and Environmental Engineering, Soongsil University, Seoul 156-743, Korea

\*\*Department of Mechanical and System Design Engineering, Hongik University, Seoul 121-791, Korea

(Received 18 September 2010 • accepted 27 October 2010)

**Abstract**—Surface-based control of melt crystallization of ibuprofen (IBU) is reported. The substrates in the present study included glass, flat Au, and laser-patterned Au. The IBU crystal morphologies were regulated depending on the surfaces where IBU crystallization was induced, and spherical, sunflower-like, and dendritic morphologies were obtained. Especially, the dendritic morphology of a large surface area was observed on the novel laser-patterned surfaces. Three-dimensionally tortuous Au structures were achieved by a 532 nm Nd : YAG laser, of which Gaussian beam profile was reshaped into a flat-top contour using a custom-designed diffusing system. Also, the effect of poly- $\epsilon$ -caprolactone was analyzed as a crystallization modulating additive to fine-tune the IBU crystal morphologies. The IBU crystallization behaviors as well as the laser patterning processes are described as a part of the ongoing efforts to develop a general strategy to utilize heterogeneous nucleation and directional growth to control the crystallization of important organic compounds, such as active pharmaceutical ingredients.

Key words: Crystallization, Ibuprofen, Dendrite, Laser, Patterning

### INTRODUCTION

Control in crystallization is often manifested in the changes of crystal orientations and shapes. Orientational regulation originates from the interactions that crystals experience during heterogeneous nucleation, self-assembly, and compliance with external fields [1-3]. It is an especially important strategy to modify macroscopic properties of the structures formed with a multitude of crystals. Shapes of single crystals are usually determined by the relative surface energy that each surface holds under specific crystallization conditions, while the kinetics of crystallization can be modified by additives in such a way that the preferentially formed surfaces are revised [4,5].

The overall crystal morphologies of polycrystalline materials are determined by the combination of orientations and shapes of constituent single crystals. Also, directional growth from nuclei or seeds can be a straightforward method to regulate the overall crystal morphology, if sequential crystallization is enabled, as opposed to spatially simultaneous crystallization [4]. Unusually well-controlled crystal morphologies are often found in biologically crystallized materials, where heterogeneous nucleation is utilized in conjunction with biomacromolecular additives [6].

In the present study, crystal morphologies of ibuprofen (IBU), a model pharmaceutical compound, were regulated, inspired by the principles of biological crystallization. (Note that the morphologies of pharmaceutical materials are of critical importance because they are closely related to the drug delivery as well as dosage form processing [7].) Specifically, melt crystallization of IBU was investigated to understand the effects of novel laser-patterned surfaces. Also, the role of a polymeric additive, poly- $\epsilon$ -caprolactone (PCL), was explored to develop synergistic capabilities in crystallization reg-

ulation.

### EXPERIMENTAL

IBU crystallization was performed via melt recrystallization. IBU powder (Sigma, 98%; m.p. 76 °C) was originally in about 100  $\mu$ m size, and ca. 1 mg IBU was recrystallized in each experiment. The IBU microcrystals were piled up at the center of each substrate occupying ca. 2 mm  $\times$  2 mm. The system temperature increased to 80 °C with a heating rate 10 °C/min using a hot stage (Linkam, TST350). After 2 min at 80 °C, the system was cooled to room temperature through natural cooling. The recrystallization process was followed by optical microscopy (OM) (Olympus, BX51). The substrates, where the recrystallization occurred, were either glass or Au surfaces. Glass substrates were prepared by cleaning microscope slides (Superior, Marienfeld) by washing with acetone or absolute ethanol.

Au substrates were of two different types. Ultra flat Au surfaces (Au-Flat) were prepared by using a Si wafer as a template. [8] About a 6  $\mu$ m-thick Au layer was sputter-coated (Cressington Sputter coater 108) on a Si wafer (Buycemi; Suwon, Korea) that had been thoroughly cleaned by successively washing with acetone, absolute ethanol, and deionized water. Then, the Au part was glued on a clean glass slide using a small amount of adhesive (Norland products, Inc., Norland optical adhesive 81; Cranbury, USA), and it was delaminated from the Si wafer to expose a highly flat Au surface.

Three dimensionally patterned Au surfaces (Au-Laser) were prepared by treating Au-Flat with a 532 nm laser (5 ns pulse duration, 10 Hz repetition rate), obtained from a frequency doubled, Q-switched Nd : YAG laser source (Quantel, Brilliant; Bozeman, USA) (Fig. 1(a)). Frequency doubling from 1,064 nm to 532 nm was achieved by using a potassium titanyl phosphate (KTP) crystal, and beam divergence was 0.5 mrad. To increase the spatial homogeneity of the laser, a diffusing system was used that had been constructed by

<sup>†</sup>To whom correspondence should be addressed.

E-mail: iwkim@ssu.ac.kr

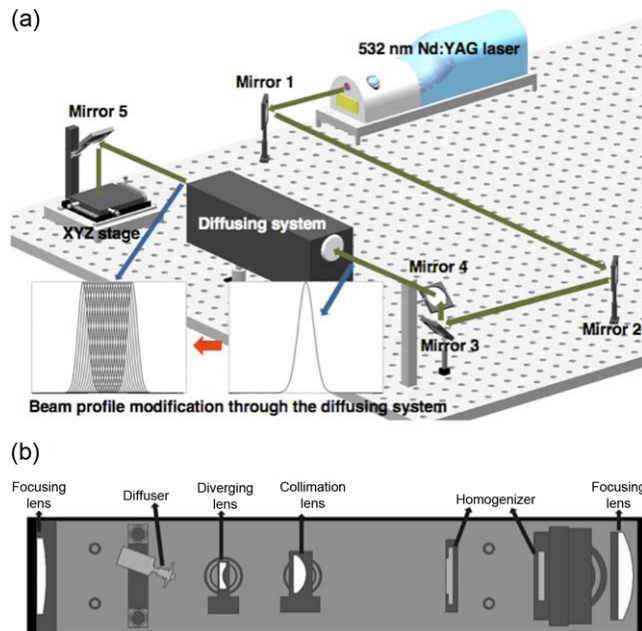


**Fig. 1.** (a) The 532 nm Nd : YAG laser setup used in the present study with schematic representation of beam profile modification through the diffusing system. (b) Details of the diffusing system constructed with a diffuser, a homogenizer, and multiple lenses.

combining a diffuser, a homogenizer, and various lenses (Fig. 1(b)). [9] The diffusing system induced multiple overlapping of the originally Gaussian laser beam profiles to ultimately generate a “flat-top” beam contour enclosing 8 mm×8 mm area. Average power and beam profiles were measured by a power meter (Gentec-EO, SoLo PE; Quebec, Canada) and a beam profiler (Gentec-EO, BeamMap2; Quebec, Canada), respectively. After the laser treatment, Au-Laser surfaces were examined using optical and atomic force microscopy (Park Systems, XE-100). OM was attempted in a reflection mode, and atomic force microscopy (AFM) was in a non-contact mode using an Si cantilever (Park Systems, NSC15). OM images were analyzed by ImageJ (National Institutes of Health, version 1.43u),

and AFM images were processed with XEI (Park Systems, version 1.7.1).

Poly- $\epsilon$ -caprolactone (PCL: Aldrich,  $M_w$ ~14,000; m.p. 60 °C) was also used as an additive for the IBU crystallization. PCL was spin-coated on glass or Au-Flat before IBU loading to ensure homogeneous mixing during IBU melting and recrystallization. The spin-coating was for 10 sec at 1,000 rpm (Dong Ah Trade Corp., ACE-1020S) by using a 5 mM solution in ethyl acetate (Samchun Chemicals, 99.5%). In addition, some samples of Au-Flat spin-coated with PCL were treated with the 532 nm Nd : YAG laser to generate Au-Laser coated with PCL.

## RESULTS AND DISCUSSION

Au-Flat substrate is shown in Fig. 2 with representative OM and AFM images. The OM image (Fig. 2(a)) was taken in a reflection mode, only showing homogeneous surface displaying bright specular reflection, and the AFM image (Fig. 2(b)) was taken in an AC mode, displaying a 10  $\mu$ m×10  $\mu$ m area that possessed root mean squared (RMS) roughness ca. 0.2 nm. Note that the Si wafer, used as a template for the Au-Flat formation, possessed RMS roughness less than 0.1 nm. When a PCL thin layer was spin-coated, the OM observation displayed an equally featureless surface, confirming homogeneously distributed PCL additive molecules on Au-Flat.

Au-Laser substrates were formed by treating Au-Flat with the 532 nm Nd : YAG laser, as described in the experimental section. The extent of laser treatment could be tuned by varying laser power density and pulse numbers (pulse duration 5 ns, pulse repetition rate 10 Hz). Also, it was possible to pre-coat PCL additives on Au-Flat before the laser treatment because PCL is transparent for the 532 nm laser. Fig. 3 shows the dramatic alteration of Au-Flat induced by the laser treatment. While the entire Au-Flat surface reflected light in a specular manner (Fig. 2(a)) showing the homogeneously bright image under the reflection mode of OM, the laser treated region of Au-Laser lost the specular characteristics to have diffuse reflection. This made it possible to identify the laser patterned area in the OM micrographs as dark spots. The changes of the Au surfaces are shown in Fig. 3 as the pulse numbers of the laser (0.39 W/cm<sup>2</sup>) increased: pulse numbers 5, 10, and 20 for Fig. 3(a), 3(b), and 3(c).

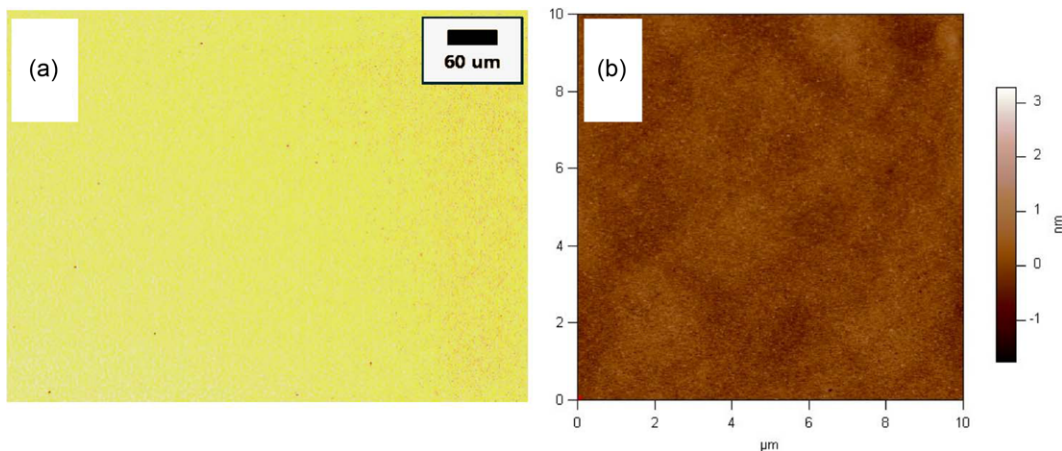


**Fig. 2.** OM (a) and AFM (b) images of the ultra flat Au surfaces (Au-Flat). Bright specular reflection was homogeneously observed in (a), and RMS roughness was determined as ca. 0.2 nm in (b).

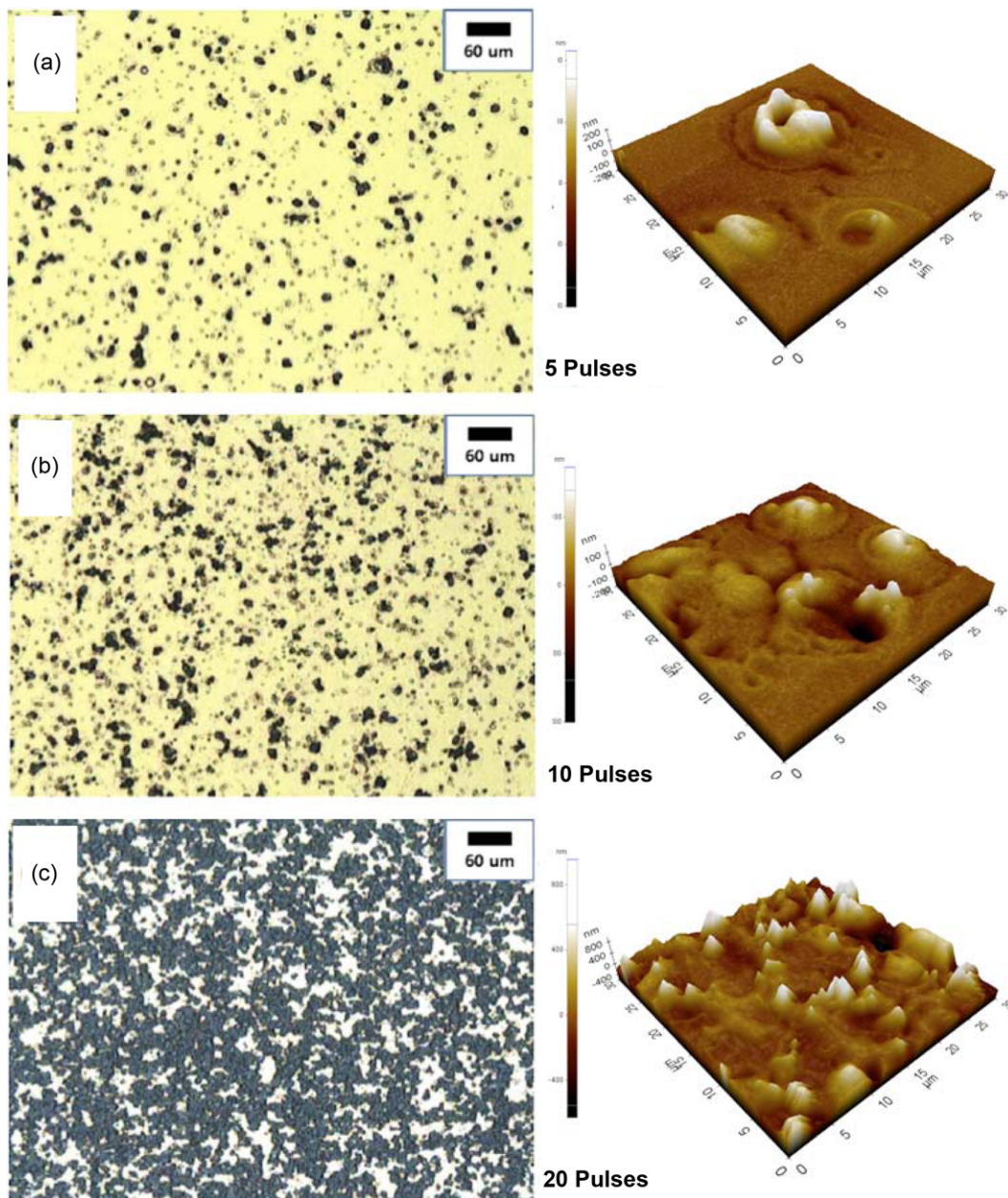


Fig. 3. OM (left) and AFM (right) images of the laser patterned Au surfaces (Au-Laser). Changes from Au-Flat are shown as a function of pulse numbers: (a) 5, (b) 10, and (c) 20 pulses at  $0.39 \text{ W/cm}^2$ . These particular cases were when PCL was coated on Au.

OM images are shown on the left side, and AFM images on the right. OM images clearly display the decrease of the flat and brightly reflecting region along with the increase of laser pulse numbers. AFM images indicated that the effects of laser treatment were manifested as the three-dimensional feature formation. Initially, the effect of laser treatment was spatially isolated as the formation of crater-like morphology (Fig. 3(a)). As the pulse numbers of the laser increased, the laser-affected regions started to overlap to eventually form distinctively sharp and tortuous three-dimensional patterns (Fig. 3(c)). Also shown in Fig. 4 is the quantitatively measured area affected by the laser treatment as the laser power density and pulse numbers were varied. Fig. 4(a) shows the increase of the laser treatment effect along with the increase of the laser power density. Note

that about  $0.16 \text{ W/cm}^2$  was the threshold power density to start any alteration of the Au surface, when 20 laser pulses were applied. Fig. 4(b) shows the increase of the laser treatment effect along with the increase of the laser pulse numbers at  $0.39 \text{ W/cm}^2$ . Note that the affected area increased quite steadily up until 10 pulses, and the increase seemed faster between 10 and 20 pulses, which coincided with the onset of the noticeable overlap of the laser-affected spots.

While the entire areas shown in OM images (Fig. 3) were irradiated by the 532 nm laser ( $0.39 \text{ W/cm}^2$ ) that encompassed  $8 \text{ mm} \times 8 \text{ mm}$ , only a fraction of regions were affected since the power density of  $0.39 \text{ W/cm}^2$  was not enough to start to melt Au globally. The small affected spots well dispersed in the entire irradiated area were achieved because the local deviation from the uniform “flat-top”

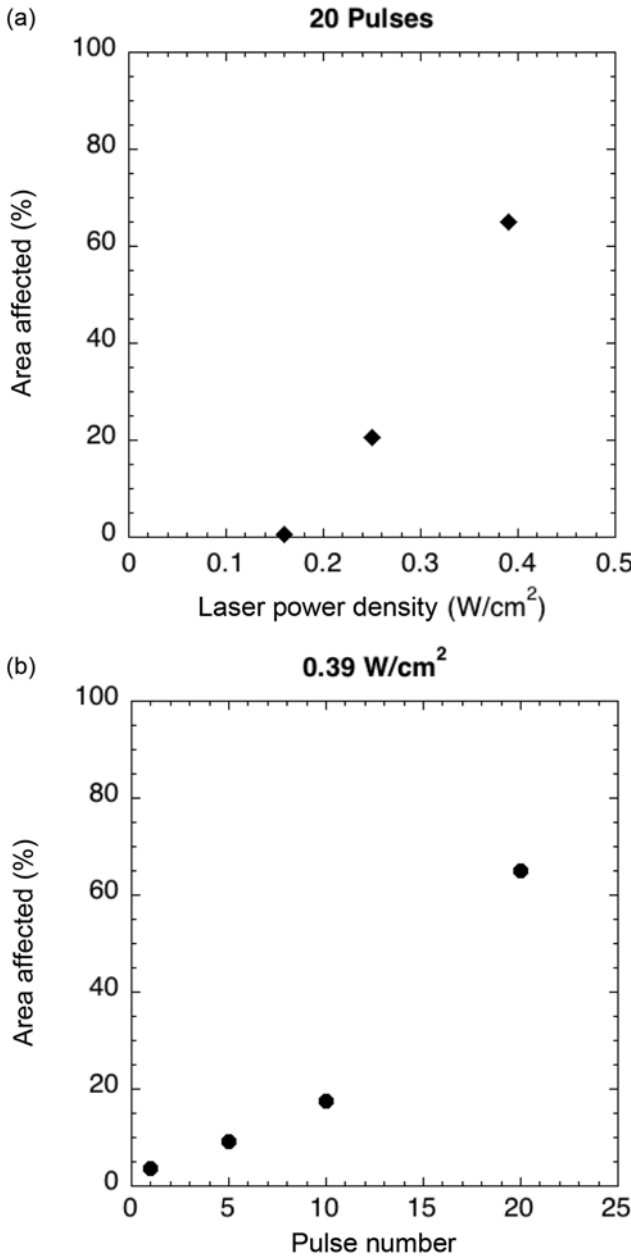


Fig. 4. Variations of laser patterned area when (a) laser power density and (b) pulse numbers were changed.

beam profile was utilized for the Au patterning. Simulation of heat transfer during the laser patterning is under investigation to predict the maximum surface temperatures along with the variation of laser power density and pulse numbers, and it will be reported elsewhere.

Melt crystallization of IBU was performed on glass, Au-Flat, and Au-Laser to probe the effects of the substrate structures on the IBU nucleation and growth. On the glass substrate, IBU powders melted to form spherically shaped droplets probably to reduce the interfacial area of the melt. The IBU melt was amorphous, and it did not show birefringence under cross-polar conditions. After 2 h, the spherically shaped IBU (ca. 1.5 mm) started to show faint birefringence, indicating the initiation of crystallization (Fig. 5(a)). Some small non-

birefringent amorphous region was also present at the same time. After 3 days, the overall shape of the round crystal was largely retained, and the birefringence became stronger (Fig. 5(b)). On the Au-Flat substrate, the initial IBU melt spread more freely to occupy larger area reflecting different interfacial interactions experienced by IBU. After 10 h, a round seed-like region (ca. 1.1 mm) formed, showing faint birefringence under cross-polar conditions, and needle-shaped crystals were almost immediately branching out from the surface of the round seed into the amorphous region (Fig. 5(c)). Dendritic structures were formed within 5 min via continued generation of crystal branches (Fig. 5(d)). Finally, a Au-Laser substrate, formed by treating Au-Flat with 20 pulses of 0.39 W/cm<sup>2</sup> Nd : YAG laser, was selected for IBU crystallization, because of its distinctive surface structure (Fig. 3(c)) as well as the patterned area over 50% (Fig. 4). On the Au-Laser substrate, the initial IBU melt spread appeared similar to that on Au-Flat. After 5 h, small crystalline region (ca. 0.1 mm) formed, and needle-shaped crystals almost immediately branched out from the initially observed region (Fig. 5(e)). Substantial differences existed between the IBU crystallization behaviors on Au-Flat and Au-Laser. The seed region on Au-Laser, where the needle formation started, was only a tenth size of the seed formed on Au-Flat. Also, the IBU crystal branches on Au-Laser appeared about 50  $\mu$ m width pseudo-plates assembled by the bundles of micro-needles (Fig. 5(f)), while those on Au-Flat were in a typical dendrite shape. From these observations on three different substrates, it was obvious that the amorphous glass substrate did not contribute to the rapid and directional growth of IBU crystals that were observed at least partly on Au substrates. Also, a three-dimensionally patterned Au-Laser substrate was effective in facilitating the directional growth to form the needle-shaped crystals of the large surface area nearly exclusively, without generating the round IBU crystals observed both on glass and Au-Flat. These behaviors were confirmed in multiply repeated independent experiments. While the exact mechanism of the controlling effects of Au-Laser is under investigation, we speculate that the three-dimensionally tortuous surface features are influential in modifying the nucleation behavior of IBU crystals in a similar way to the graphoepitaxy [10].

Melt crystallization of IBU (m.p. 76 °C) was also performed in the presence of PCL (m.p. 60 °C) on glass, Au-Flat, and Au-Laser to investigate the combined effects of the PCL additive and the substrate structures. PCL had been spin-coated on the substrates before IBU melt recrystallization. On the glass substrate coated with PCL, initial melting and recrystallization behavior was similar to that without PCL. After 5 h, however, about 20% of the IBU formed more irregularly shaped structures than simple spherical forms (Fig. 6(a)). In time, other regions also developed further into the aggregation of platy needle crystals (Fig. 6(b)); similar behavior was not seen when PCL was absent. On the Au-Flat substrate coated with PCL, a sunflower-like overall morphology was again observed as was without PCL. However, the size of the seed part was about half in its diameter (ca. 0.5 mm), as shown in Fig. 6(c), compared to that on Au-Flat without PCL. Also, the crystal branches appeared to populate more densely (Fig. 6(d)). On the Au-Laser substrate coated with PCL, the overall crystal assembly was remarkably similar to those on the same substrate but without PCL. The needle-shaped crystals seemed to branch out from the ca. 0.1 mm center region (Fig. 6(e)), and the multiple needles assembled to form each branch

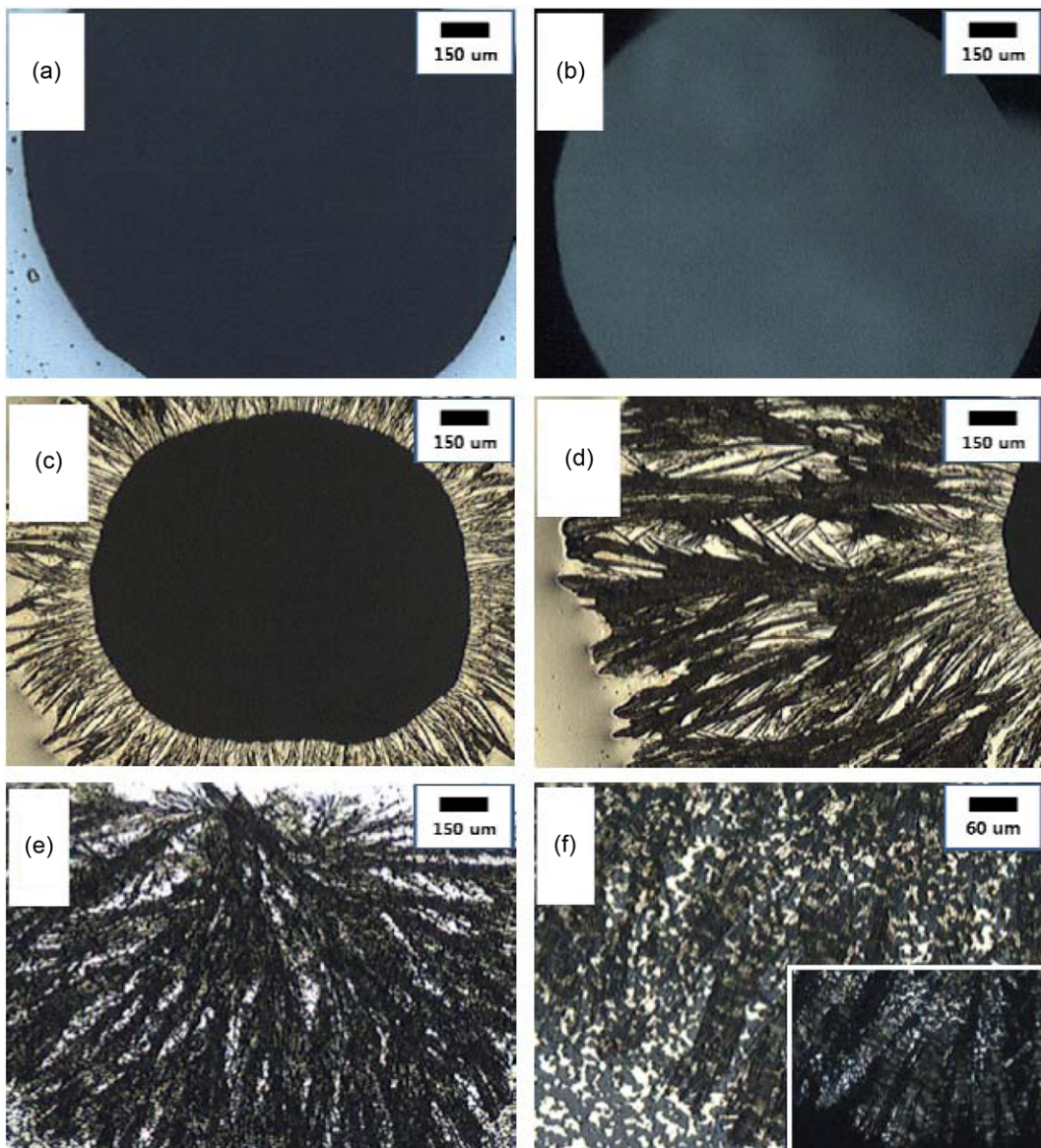


**Fig. 5.** Glass induced spherically shaped IBU crystals: after (a) 2 h and (b) 3 days. Au-Flat formed sunflower-like IBU crystals on Au-Flat (c) after 10 h; further branching generated dendritic morphology (d). Au-Laser prompted dendritic IBU crystal formation in general (e) after 5 h; more detailed view (f) of individual branches reveals pseudo-plates formed by multiple needles. Micrographs of (b) and the inset of (f) were taken under cross-polar conditions for clear representation.

as pseudo-plates (Fig. 6(f)). From these observations on three different substrates, it was clear that the PCL had exerted considerable effects in modifying the melt crystallization of IBU. The effects were most significant with glass substrate and least expressive with Au-Laser, which was probably related to the crystallization controlling ability of the substrates in the present study. The exact nature of the PCL-IBU interaction is under investigation in terms of crystallization kinetics.

## CONCLUSIONS

Melt crystallization of IBU was successfully controlled with different types of substrates: glass, ultra-flat Au, and three-dimensionally patterned Au. The ultra-flat Au surface was obtained by using

an atomically flat Si wafer as a template, and the three-dimensionally patterned Au surface was processed by treating the flat Au surface with a 532 nm Nd : YAG laser [8,9]. These model substrates were designed to regulate the heterogeneous nucleation of IBU at the interfaces by utilizing amorphous, flat crystalline, and three-dimensionally tortuous crystalline surfaces. The amorphous glass acted to form droplet-shaped IBU crystals on a millimeter-scale. The flat crystalline Au surface induced the formation of micro-needles of IBU crystals, although it did not entirely suppress the large round IBU crystal formation. The three-dimensionally tortuous crystalline Au surface formed the micro-needles of IBU crystals nearly exclusively, and it completely suppressed the large round IBU crystal formation. The crystallization control exerted by these substrates was also combined with the effect of a polymeric additive, PCL. It was a fairly

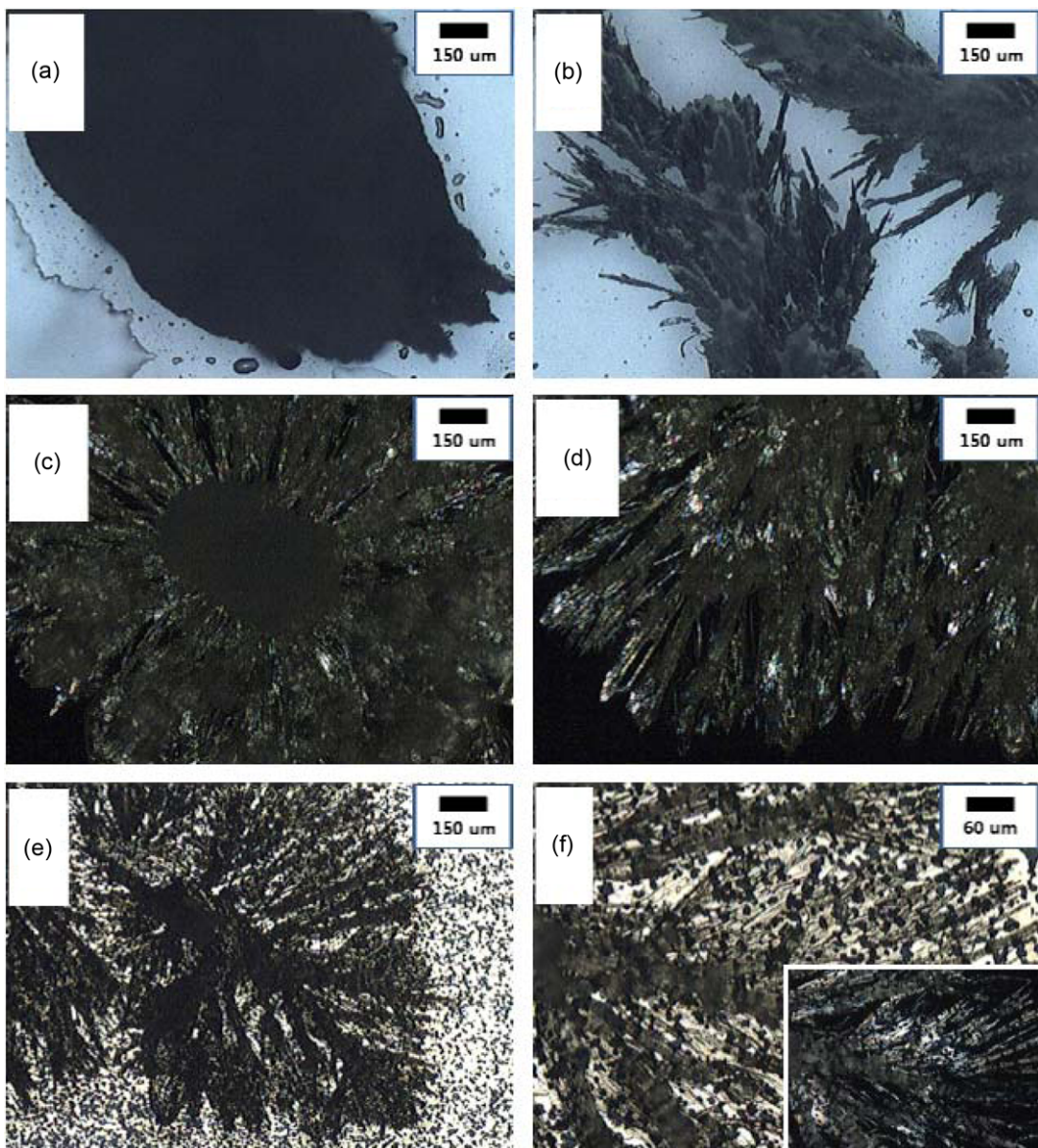


**Fig. 6. IBU crystallization in the presence of PCL pre-coated on the substrates.** Glass induced irregularly shaped structures (a) after 5 h; other regions eventually became the aggregation of platy needle crystals (b) after 3 days. Au-Flat formed IBU crystals of sunflower-like morphology (c) after 7 h; details of needle morphology are shown in (d). Au-Laser prompted IBU crystal formation in a similar manner without PCL (e) after 5 h; details of needle morphology are shown in (f). Micrographs of (c), (d), and the inset of (f) were taken under cross-polar conditions for clear representation.

effective additive to form needle-shaped crystals when used for the glass substrate, but its effect was marginal with Au surfaces probably because of the greater effects of the substrates. The control of the crystallization behavior using designed surfaces is a recurrent and effective methodology [1,3]. In the present study, we demonstrated a relatively quick and simple method of the laser irradiation to reshape Au substrates, and these were used to regulate the crystallization of an important pharmaceutical material, IBU. Further efforts are being made to make the current method a part of the more general strategy to fine-tune the structures of crystals. Eventually, we expect that the controlled formation of microneedles of drug crystals on surfaces could become the key technology for the drug delivery utilizing microneedle patches [11].

## ACKNOWLEDGEMENT

This research was supported by Basic Science Research Program through the National Research Foundation of Korea (NRF) funded by Ministry of Education, Science, and Technology (2009-0075243).

## REFERENCES

1. J. Aizenberg, A. J. Black and G M. Whitesides, *J. Am. Chem. Soc.*, **121**, 4500 (1999).
2. M. Li, H. Schnablegger and S. Mann, *Nature*, **402**, 393 (1999).
3. I. W. Kim, R. E. Robertson and R. Zand, *Adv. Mater.*, **15**, 709 (2003).

4. J. W. Mullin, *Crystallization*, Butterworth-Heinemann, Oxford (2001).
5. J.-H. Kim, S. M. Song, J. M. Kim, W. S. Kim and I. H. Kim, *Korean J. Chem. Eng.*, **27**, 1532 (2010).
6. S. Weiner and L. Addadi, *J. Mater. Chem.*, **7**, 689 (1997).
7. R. I. Mahato, *Pharmaceutical dosage forms and drug delivery*, CRC Press, Boca Raton, FL (2007).
8. J. J. Blackstock, Z. Li and G. Jung, *J. Vac. Sci. Technol. A*, **22**, 602 (2004).
9. J. Lee, J. Park, J.-H. Hwang, S. Park and H. Chung, *Proceedings of Joint International Symposia on 3<sup>rd</sup> Micro & Nano Technology and Micro/Nanoscale Energy Conversion & Transport*, 143 (2010).
10. E. I. Givargizov, *J. Cryst. Growth*, **310**, 1686 (2008).
11. S. P. Sullivan, D. G. Koutsonanos, M. del P. Martin, J. W. Lee, V. Zarnitsyn, S.-O. Choi, N. Murthy, R. W. Compans, I. Skountzou and M. R. Prausnitz, *Nat. Med.*, **16**, 915 (2010).